Journal of Catalysis **210,** 149–159 (2002)
doi:10.1006/jcat.2002.3632

Structured Au/FeO_x/C Catalysts for Low-Temperature CO Oxidation

Dmitri A. Bulushev,* Lioubov Kiwi-Minsker,*,[1] Igor Yuranov,* Elena I. Suvorova,†
Philippe A. Buffat,† and Albert Renken*

*LGRC, †CIME, Swiss Federal Institute of Technology, CH-1015 Lausanne, Switzerland

Received January 31, 2002; revised April 3, 2002; accepted April 4, 2002

Innovative structured catalysts based on nanoparticles of gold supported on activated carbon fibers (ACF) in the form of woven fabrics are presented for low-temperature CO oxidation. Gold was deposited by adsorption from aqueous solution of ethylenediamine complex $[Au(en)_2]Cl_3$ followed by reduction in hydrogen. The catalysts were studied under transient reaction conditions and characterized by high-resolution transmission electron microscopy (HRTEM) and X-ray energy dispersive analysis (EDS). HRTEM-EDS shows that gold is present on the surface of Au/ACF catalyst in the form of metallic particles with sizes of ∼2.5–5 and ∼30–50 nm. A predeposition of iron oxide on the ACF was beneficial for the Au dispersion and catalytic activity in CO oxidation. Gold particles in the Au/FeO_x/ACF samples were not in direct contact with the Fe_2O_3 phase and their size was smaller than without doping by iron oxide. The mechanism of catalyst formation, its morphology, and the influence of preparative conditions are discussed. The activity of Au/FeO_x/ACF was substantially higher as compared to Au/Al_2O_3 and Au/FeO_x/Al_2O_3 catalysts. A reductive pretreatment with H_2 was necessary to activate the catalyst, but the activity decreased rapidly in CO/O_2 atmosphere. Addition of hydrogen or water vapors to the reaction mixture increases the catalyst activity.

Key Words: **CO oxidation; nanoparticles of gold; structured catalysts; iron oxide; deactivation; activated carbon fibers; fuel cells; high-resolution electron microscopy; transient-response method.**

1. INTRODUCTION

Supported catalysts containing nanoparticles of Au have the unique property of oxidizing CO at low temperatures (200–300 K). These catalysts are attractive for purification of contaminated air and for utilization in CO detectors, protective gas masks, and CO_2 lasers (1–4). The remarkable catalytic activity of supported gold catalysts with respect to the bulk metallic Au is assigned to the presence of highly dispersed gold particles (2–5 nm). The mechanism of reactant activation is still a controversial matter in spite of extensive studies during the last decade (4). Properties of the supported Au catalysts were found to depend on the method of preparation, calcination, and pretreatment procedure (1–4). Coprecipitation and deposition–precipitation are more adequate methods of preparation than is impregnation (1, 4) giving smaller Au particles and higher catalytic activity. Gold dispersed over iron oxide is reported to be among the most active catalysts for CO oxidation.

The catalytic preferential CO oxidation to CO_2 performed in the presence of hydrogen (PROX process) found recently an important application in hydrogen purification in fuel cell technology (5–10). The activity and selectivity of Au/FeO_x was comparable with that of the Pt/Al_2O_3 catalyst even at a temperature 120 K lower (5, 7). The Au particularity of oxidizing CO much faster than H_2 is the basis of the improved catalytic performance. Additionally, CO was shown to inhibit H_2 oxidation (9), but by other authors (10) the acceleration has been also reported.

The reactor design is important for the optimized fuel cell performance. Recently, we reported the preparation methods of structured catalysts based on silica fiber woven fabrics for catalytic combustion (11, 12) and benzene gas-phase hydroxylation (13), as well as for three-phase liquid-phase hydrogenation reactions (14, 15). Activated carbon fibers (ACF) in the form of woven fabrics have been used as supports for noble metal deposition and tested as catalysts in liquid-phase hydrogenation (16, 17) and gas-phase selective reduction of NO_x (18). A high specific surface area (SSA) and low weight of the ACF supports are advantageous for their application in the PROX process, if high activity/selectivity is achieved. The ACF-based catalysts are easy to handle and to adapt to any reactor geometry and gold could be recovered from the spent catalyst by burning off the carbon.

Gold supported on activated carbon was reported to be catalytically active in hydrochlorination of ethyne (19) and some selective liquid-phase oxidation reactions (20, 21), but it has not been tested in CO oxidation. The present work was aimed at the development of structured catalysts consisting of nanoparticles of Au supported on the ACF woven fabrics for low-temperature CO oxidation. Influence of the ACF support modification by iron oxide as well as the catalyst pretreatment on activity and stability with time-on-stream was investigated regarding the catalyst morphology. The transient-response method was applied to follow the

[1] To whom correspondence should be addressed. Fax: +41-21-693-31-90. E-mail: lioubov.kiwi-minsker@epfl.ch.

0021-9517/02 $35.00

evolution of activity after different pretreatments. The catalytic properties of the Au/ACF were compared with granulated Au/Al_2O_3, $Au/FeO_x/Al_2O_3$, and Au/FeO_x. High-resolution transmission electron microscopy (HRTEM) and X-ray energy dispersive spectroscopy (EDS) were used to study the catalyst morphology and chemical composition in details.

2. EXPERIMENTAL

2.1. Catalyst Preparation

2.1.1. Materials. Gold(III) chloride hydrate $HAuCl_4 \cdot aq$, iron(III) nitrate $Fe(NO_3)_3 \cdot 9H_2O$, ethylenediamine $NH_2C_2H_4NH_2$ (en), and aqueous ammonia (28 wt%) were of p.a. quality and purchased from Fluka (Buchs, Switzerland). $[Au(en)_2]Cl_3$ was synthesized from $HAuCl_4 \cdot aq$ and ethylenediamine as described elsewhere (22). Deionized water was used during the catalyst preparations.

Granulated alumina with a specific surface area (SSA) of 140 m^2/g (Engelhard) and activated carbon fibers (ACF) in the form of woven fabrics (AW1101, KoTHmex, Taiwan Carbon Technology Co.) were used as starting materials for the support's preparation. The alumina was crushed and sieved to obtain 0.25- to 0.5-mm grains. The surface functionality of the activated carbons is known to be regulated by different pretreatments (23, 24). The ACF support was boiled in 15 vol% HNO_3 for 1 h, then rinsed with water and dried in air.

2.1.2. Modification of the supports by iron oxide. Iron oxide was deposited on alumina via an incipient wetness impregnation with 2.2 M $Fe(NO_3)_3 \cdot 9H_2O$ solution, followed by drying in air at room temperature and calcination at 823 K during 4 h.

For the preparation of ACF modified by iron oxide (FeO_x/ACF) the ACF fabric was immersed into aqueous solution of $Fe(NO_3)_3 \cdot 9H_2O$ (10 wt%), which was hydrolyzed by two methods: (i) by slow addition of ammonia until pH 3 under vigorous stirring for 1 h; (ii) by using urea as a precipitating agent under vigorous stirring at 353 K until the solution reached pH 3.5. Then the ACF fabric was rinsed with water and the operation of iron hydroxide deposition was repeated if necessary to obtain the higher iron loading (10.8 wt%). Finally, the ACF fabrics were boiled in water for 1 h and dried in air at room temperature.

2.1.3. Preparation of gold catalysts. Two different gold precursors were used for the Au deposition depending on the support:

(a) *Gold deposition on the alumina and FeO_x modified alumina* was carried out by adsorption from $HAuCl_4$ aqueous solution. The grains (2 g) were immersed into 20 ml of the 0.1 wt% $HAuCl_4 \cdot aq$ solution and the mixture was stirred for 4 h. Then, the grains were recovered by filtration, washed with water, and dried in air at room temperature.

(b) *Gold deposition on the ACF supports* was carried out from aqueous solution of ethylenediamine complex $[Au(en)_2]Cl_3$ with initial concentrations varying from 0.05 to 0.2 wt%. The ACF and FeO_x/ACF fabrics (2 g) were immersed in the $[Au(en)_2]Cl_3$ solution (20 ml), which was stirred for 3 h. After the adsorption the fabrics were rinsed in water and dried in air at room temperature.

2.2. Catalyst Characterization

The loading of Fe and Au were measured by atomic absorption spectroscopy (AAS) using a Shimadzu AA-6650 spectrophotometer with an air–acetylene flame. For the analysis the oxide-based catalysts were dissolved in hot aqua regia containing several drops of HF. The ACF-based catalysts before dissolving were heated in air at 973 K for 2 h in order to burn out the carbon. The results of chemical analysis are presented in Table 1.

The surface morphology of the supports and the catalysts was investigated via scanning electronic microscopy (JSM-6300F, JEOL) and high-resolution transmission electron microscopy (Philips CM300UT FEG with a 300-kV field emission gun, 0.65-mm spherical aberration, and 0.17-nm resolution at Scherzer defocus). Chemical analysis was performed with X-ray energy-dispersive analysis (EDS, INCA, Oxford) with probes 2–8 nm in diameter corresponding roughly to the size of Au particles. Pieces of the catalysts, thin enough for electron transparency, were placed on a TEM carbon film supported on a Cu grid.

A contribution of iron to the ED spectra came not only from the catalyst but also from the backscattered electrons

TABLE 1

Catalytic Activity in CO Oxidation at 303 K after Different Times-on-Stream[a]

Catalyst[b]	Catalytic activity (mol CO × 10^3 g_{Au}^{-1} s^{-1})		
	Initial (0.3–1 min)	30 min	120 min
0.5% Au/FeO_x/ACF (1.8% Fe)	>20	0.8–1.6	0.36–0.50
0.05% Au/FeO_x/ACF (1.8% Fe)	>20	0.8–1.0	0.30–0.50
1.3% Au/FeO_x/ACF (4.5% Fe)	>4	0.26	0.12
0.9% Au/FeO_x/ACF (10.8% Fe)	1.1	0.05	—
0.12% Au/ACF	11	0.09	—
0.6% $Au/FeO_x/Al_2O_3$ (6.2% Fe)	>1	0.10	—
0.5% Au/Al_2O_3	0.06–0.09	0.01–0.02	—
0.5% Au/FeO_x/ACF (1.8% Fe) at 243 K	>10	0.9	—

[a] 1 vol% CO; $O_2/CO = 5$. All samples were prereduced in H_2 at 573 K.
[b] The composition of the catalysts was determined by chemical analysis (AAS).

heating the objective lens pole pieces. Therefore, for quantitative analysis blank experiments were performed with the carbon film without any sample. The signal obtained was then subtracted during the measurements of the catalysts. The HRTEM images were recorded on a Gatan 797 slow-scan CCD camera (1024 × 1024 pixels) and processed with the Gatan Digital Micrograph 3.4.4 software to measure distances and angles between atomic planes.

The phase identification of the particles was carried out by computing the fast Fourier transform diffractograms of the HRTEM images on a nanometer scale. An interpretation of the HRTEM results was performed with the JEMS software package (25) using the electron-optical parameters and structural data for iron oxides (FeO, Fe_2O_3), metallic iron, and gold (26).

The elemental surface composition of the ACF support was studied by X-ray photoelectron spectroscopy (XPS) using an Axis Ultra ESCA system (Kratos, Manchester) with monochromated Al K_α radiation (1486.6 eV) and an X-ray power of 150 W.

The specific surface area (*SSA*) of the supports and catalysts were measured using N_2 adsorption–desorption at 77 K by a Sorptomatic 1990 instrument (Carlo Erba). The samples were heated in vacuum at 523 K for 2 h before the measurements. The SSA of the samples was calculated employing the BET method. The Dollimore/Heal method was applied for the calculation of pore volume and pore-size distribution.

2.3. Catalytic Activity Measurements

A Micromeritics AutoChem 2910 analyzer provided with a plug-flow reactor was used for the transient-response studies. This setup allowed quick changing of one gas flow over the catalyst to another. All samples (the catalyst weights are indicated in the figure captions) were preheated in the reactor in pure H_2 until 573 K (5 K/min), kept at this temperature for 30 min, then quickly cooled in H_2 to room temperature. This pretreatment was necessary to activate the catalyst. After the reaction of CO oxidation, an oxidative pretreatment was performed by heating the sample in a 10-vol% O_2/He mixture with a temperature ramp of 5 K/min. After reaching 573 K, quick cooling was performed either in the same mixture or in He. The catalytic activity was measured again and the cycle was repeated. The gases used were of >99.999% purity (CarbaGas, Switzerland).

After the pretreatment, the catalyst was purged by He for 15 min at room temperature. The mixture of 1 vol% CO/5 vol% O_2/45 vol% He/49 vol% Ar with a total gas flow of 20 or 100 ml (STP)/min was used to measure the catalytic activity in CO oxidation. In the presence of H_2 (PROX process) the mixture of 1 vol% CO/1 vol% O_2/49 vol% H_2/49 vol% He was used and the activity was compared with that obtained with a mixture of 1 vol% CO/1 vol% O_2/49 vol% Ar/49 vol% He. Water was pulse injected (1 μl) via an evaporator using a syringe to study its influence on the catalytic activity.

The products in the reactor outlet were analyzed by a ThermoStar-200 quadrupole mass spectrometer (Pfeiffer Vacuum). The mass spectrometer was calibrated using gas mixtures of known compositions. The reaction temperature was controlled by a thermocouple inserted inside the catalyst bed. The CO conversion was determined as the concentration of CO_2 related to the initial CO concentration in the reaction mixture. The carbon balance was controlled during experiments. After 150 s it was within $100 \pm 2\%$. The reaction rate used as a characteristic of the catalytic activity was determined under differential conditions at conversions <0.15. Some difference in the activity of the samples taken from different places of the catalyst fabric was observed. It was explained, at least partly, by some inhomogeneity of the active-phase deposition over the ACF support.

3. RESULTS AND DISCUSSION

3.1. Characterization of the Fibrous Activated Carbon Support

As seen from the SEM image, the ACF support is woven from threads consisting of a bundle of elementary filaments (Fig. 1). The filament diameter is around 5 μm.

The N_2 adsorption–desorption measurements showed an isotherm of type I, which is characteristic for microporous

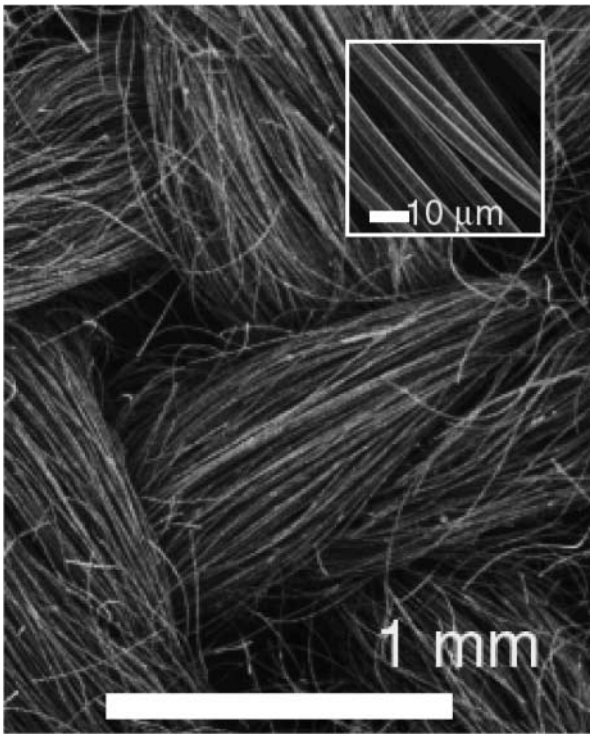

FIG. 1. Scanning electron microscopy image of the woven fabric of activated carbon fiber (ACF) support.

materials (27). The oxidative treatment with nitric acid removes impurities and changes the surface functionality by the formation of oxygen-containing groups (28). The SSA of the ACF after the acidic treatment was slightly increased from 880 to 950 m^2/g. The specific pore volume at $P/P_0 = 0.9999$ was equal to 0.58 ml/g. Most of the pores have a diameter less than 2 nm. The pores larger than 10 nm were not found. No change in SSA and pore-size distribution was observed upon iron oxide and gold deposition.

The mineral matter by weight in the ACF support was about 0.6 wt%, with silicon as the predominant component. The presence of silicon in the subsurface region was detected by XPS (surface atomic Si/C ratio ~2%) together with nitrogen and large amounts of oxygen. Carbon, silicon, and oxygen as the main components of the ACF fabrics were found by EDS, with the average bulk atomic Si/C ratio ~4%.

3.2. Catalytic Activity in CO Oxidation at Room Temperature

3.2.1. Catalyst screening. Figure 2 shows the evolution of conversion in CO oxidation with time-on-stream for different prereduced catalysts taken with the same amount of supported gold. It is seen that the conversion over the 0.5% $Au/FeO_x/ACF$ catalyst is the highest and reaches 100%.

An interaction of CO (2 vol% CO/Ar mixture) with the 0.5% $Au/FeO_x/ACF$ catalyst after standard reduction followed by oxidation (10 vol% O_2/He mixture for 15 min at room temperature) was also performed. Only traces of CO_2 ($\leq$0.01 vol%) were formed, contrary to the large amounts produced in the presence of oxygen (~1 vol%; Fig. 2). These data indicate that weakly adsorbed oxygen formed on the catalyst surface in the presence of gaseous oxygen

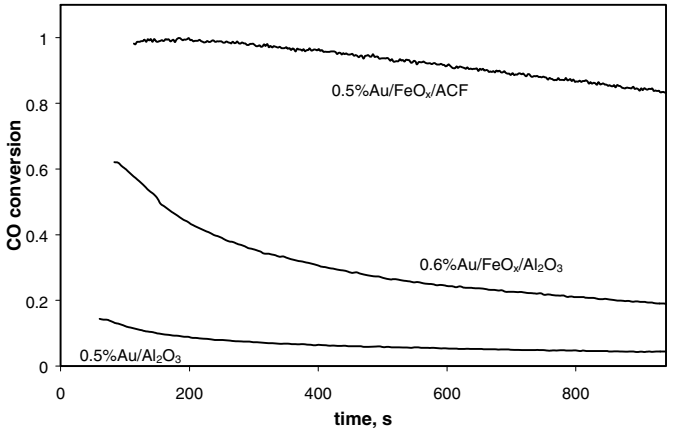

FIG. 2. CO conversion over prereduced catalysts loaded into the reactor with the same charge (0.047 g, 20 ml/min, 1 vol% CO/5 vol% O_2 with the rest Ar and He, 303 K).

was necessary for CO oxidation. These data are in line with the TAP reactor (29), temperature-programmed desorption (30), and isotopic (30) and electron spin resonance (31, 32) data obtained for different Au-containing catalysts.

To determine the reaction rate over the $Au/FeO_x/ACF$ catalysts the contact time was decreased 40 times by diminishing the catalyst charge and increasing the flow rate. The obtained values are presented in Table 1. It is seen that the activity of the Au-containing catalysts was strongly dependent on the support. Au on alumina and on FeO_x/Al_2O_3 had lower activity than on the ACF support. The ACF-based catalysts showed higher initial activity but were observed to deactivate quickly in the reaction medium.

The beneficial effect of the FeO_x addition is clearly seen from the comparison of the activities of the Au/Al_2O_3 and $Au/FeO_x/Al_2O_3$ catalysts (Fig. 2, Table 1). The FeO_x deposition considerably improves the catalytic activity. At the same time, no CO conversion was observed over the FeO_x/Al_2O_3 catalyst without gold, in agreement with Grisel and Nieuwenhuys (9, 33). The same tendency was observed for the ACF-based catalysts since the activity of the Au supported on the ACF modified by iron oxide was higher (Table 1). The activity of the FeO_x/ACF fabrics without Au was also found to be negligible at room temperature. Additionally, the Au/ACF catalyst deactivated more rapidly than the catalysts modified by iron oxide.

The activity per gram of gold of the 0.5% $Au/FeO_x/ACF$ and 0.05% $Au/FeO_x/ACF$ catalysts attained roughly the same value (Table 1). This suggests that the amount of active sites is proportional to the gold loading. The obtained activity ($0.36–0.5 \times 10^{-3}$ mol of CO $g_{Au}^{-1}\,s^{-1}$) was comparable with the one reported in the literature for the Au/FeO_x catalysts, being in the range of $0.11–0.49 \times 10^{-3}$ mol of CO $g_{Au}^{-1}\,s^{-1}$ (5, 34–36). The temperature does not affect significantly the activity of the 0.5% $Au/FeO_x/ACF$ catalyst (Table 1), indicating a very low activation energy of the reaction.

To investigate the influence of the active-phase loading on the specific activity, the 1.3% $Au/FeO_x/ACF$ catalyst with the same Fe/Au atomic ratio (12.7) but 2.6 times higher Au/FeO_x content was prepared. It is seen from Table 1 that no improvement in the catalytic activity was attained. On the contrary, the catalyst demonstrated three to five times lower activity compared with the 0.5% $Au/FeO_x/ACF$ catalyst. An increase in the iron concentration to 10.8 wt% (0.9% $Au/FeO_x/ACF$) diminished even more the activity per gram of Au, as shown in Table 1.

3.2.2. Effect of pretreatment. The effect of pretreatment on the catalytic activity in CO oxidation is shown for the 1.3% $Au/FeO_x/ACF$ catalyst (Fig. 3). One reductive and two oxidative pretreatments were performed. It is seen that the catalyst reduced by H_2 possesses the highest initial catalytic activity, but deactivates strongly. After some time-on-stream the deactivation diminished. The initial activity of

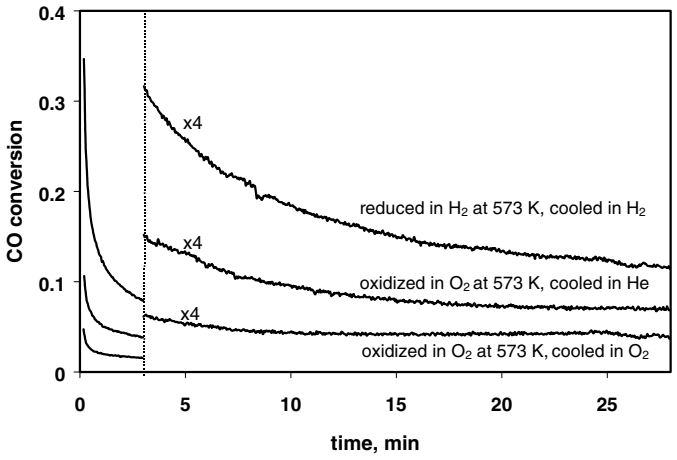

FIG. 3. CO conversion over the 1.3% Au/FeO_x/ACF catalyst (0.0057 g) on time after different pretreatments (100 ml/min, 1 vol% CO, $O_2/CO = 5$) at 303 K.

the catalyst preoxidized and cooled in O_2 was several times lower than the reduced one, but almost no deactivation was observed. The preoxidized catalyst cooled in an inert gas possessed an intermediate initial activity (Fig. 3). Similar features were found for other Au/FeO_x/ACF catalysts.

Moreover, no activity at room temperature was determined for the Au/Al_2O_3 and $Au/FeO_x/Al_2O_3$ catalysts after preoxidation. Considerable deactivation of different gold catalysts has been reported (5, 37–41). An increase in the activity after reductive pretreatment was also observed (9, 39, 42), distinguishing this pretreatment from the calcination in air at 573–673 K proposed by Haruta and co-workers (1, 34, 43). As follows from the FTIR-data the state of adsorbed CO on the oxidized and reduced gold particles differs substantially (4, 41, 42).

The deactivation presented in Fig. 3 was seen to be reversible. After the reactivation of the catalyst in hydrogen (573 K), either after intermediate oxidation (573 K) or after the reaction at room temperature, the same dependence of activity on time was observed. This fact suggests that the deactivation cannot be explained by Au sintering at room temperature but may be due to the catalyst oxidation. It is reported (44) that adsorption of oxygen on microcrystalline Au takes place at room temperature with the 1 : 1 ratio of adsorbed oxygen to surface Au atoms. An increase in the temperature to 600 K provides a higher O/Au ratio (up to 2). The presence of trivalent gold in the Au/MeO_x catalysts was detected by ^{197}Au Mössbauer spectroscopy (45, 46), XPS (37, 47), and XANES (37). Different hydroxylated species of gold, such as $Au(OH)_3$ (37) and $AuO(OH) \cdot H_2O$ (46), were also found. However, it has been claimed that metallic gold is necessary for CO activation (2, 3).

In order to understand the reasons for the catalyst deactivation, transient-response techniques were employed. Transient curves of C- and O-balance obtained during the introduction of the CO/O_2 mixture on the 0.5% Au/FeO_x/ACF catalyst after different pretreatments are shown in Fig. 4. They were normalized and compared with the normalized response curves of the Ar present in the reaction mixture. An initial accumulation of the adsorbed C and O determined by integration of the area between the Ar and products response curves is also shown by bar diagram. The adsorbed C and O atoms were related to the amount of iron atoms in the sample in spite of the adsorption that might take place also on the ACF. It is seen that the prereduced catalyst adsorbs substantial amounts of oxygen at room temperature from the reaction mixture (Fig. 4, prereduced). The main part of oxygen is adsorbed quickly since oxygen appears in the gas phase with the 0.5-min delay with respect to Ar. However, some part of oxygen may adsorb slowly, providing continuous deactivation.

The amount of adsorbed C (in the form of adsorbed CO_x) is much smaller and almost equal to the amount of C adsorbed during the reaction on the preoxidized catalyst (Fig. 4, preoxidized). The O/C atomic ratio in the adsorbed species close to 2 for the preoxidized catalyst as well as for the catalyst pretreated in the reaction (Fig. 4) is assigned mainly to the formation of carbonate (CO_3^{2-}) and/or formate species ($HCOO^-$). These species were detected by FTIRS on supported gold catalysts (34, 38, 39).

The contribution of adsorbed CO species to the total amount of adsorbed carbon-containing species seems to be small. Introducing the 2 vol% CO/Ar mixture into the preoxidized catalyst resulted in a six times lower consumption of C-containing species (C/Fe = 0.037) than did the preoxidized catalyst in the presence of oxygen (C/Fe = 0.21, Fig. 4).

The formation of the formate/carbonate species on Au/ZrO_2 was previously discussed regarding deactivation (38). The present study also indicates the possible formation of C-containing species as one of the reasons for deactivation. It is seen in Fig. 5 that the catalyst purged by He shows a 20% increase in initial conversion. The He purge seems to remove reversibly adsorbed species existing in equilibrium with the reaction mixture.

3.3. Catalytic Activity in CO Oxidation in the Presence of H_2 or H_2O

The hydrogen-rich gas used for fuel cells contains CO, O_2, H_2O, and CO_2 and traces of organic compounds. Carbon monoxide has to be removed from the stream to prevent poisoning of the electrocatalyst. It is important for the development of the catalyst for hydrogen purification from CO to know how the components of the reaction mixture influence the rate of CO oxidation. We focused therefore on the effect of water and hydrogen on the CO conversion over the 1.3% Au/FeO_x/ACF catalyst.

An introduction of excess of H_2 (49 vol%) instead of Ar into the reaction mixture does not change the initial CO

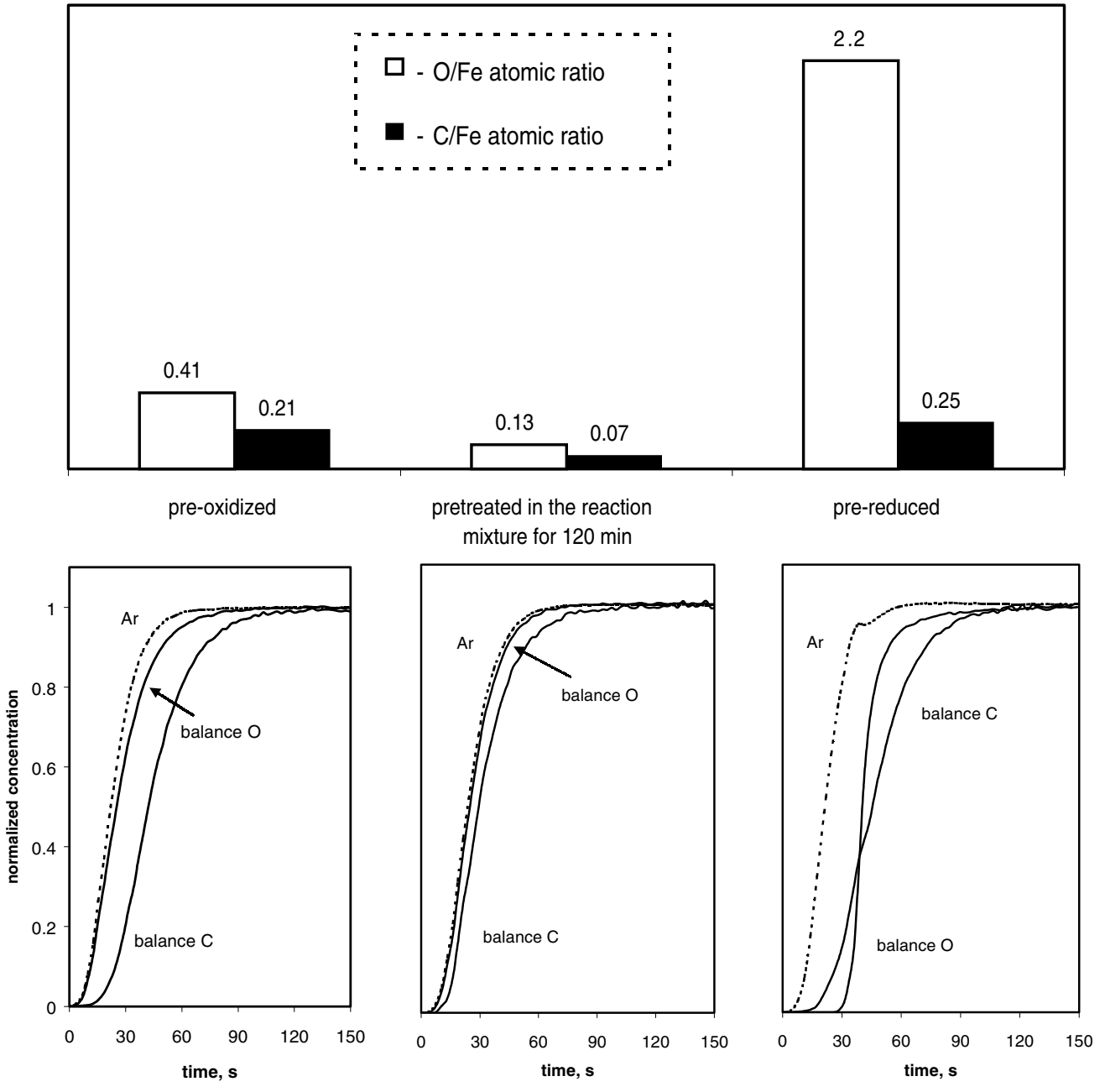

FIG. 4. Effect of the catalyst pretreatment on the carbon- and oxygen-balance response curves and the initial accumulation of oxygen and carbon atoms on the surface related to the amount of Fe atoms (bar diagram) during the CO oxidation (1 vol% CO, $O_2/CO = 5$) over 0.5% Au/FeO_x/ACF catalyst (0.047 g) at 303 K.

conversion; however, the catalyst deactivation decreases (Fig. 6). The activity after 40 min on-stream in the presence of H_2 is 1.5 times higher. The initial selectivity of the PROX process was estimated to be around 75%.

The increase in the CO conversion cannot be explained by a decrease in the oxygen concentration in the reaction mixture because of the competitive reaction of H_2 oxidation. In this case a negative reaction order toward oxygen would be observed. However only positive or zero reaction orders toward oxygen and CO are reported (2, 5, 8, 39). By FTIR spectroscopy it was seen that CO adsorbs reversibly on supported gold particles at room temperature (2, 3). Under these conditions hydrogen adsorption on gold is negligible if it takes place at all (3). Hence, hydrogen adsorption on gold particles can hardly affect CO adsorption and subsequent reaction. However, some water

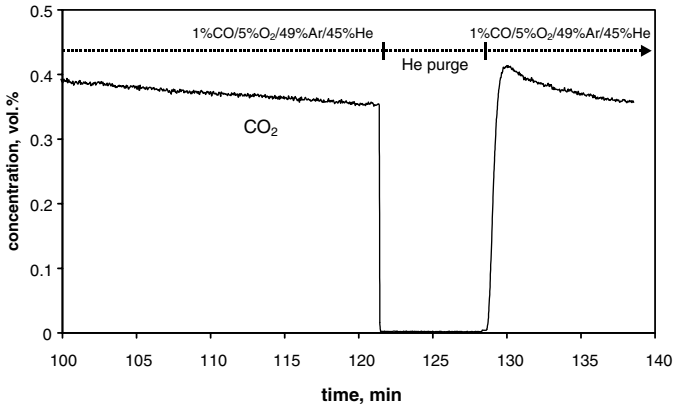

FIG. 5. Effect of the reactor purge by He on the activity of 0.5% $Au/FeO_x/ACF$ catalyst (0.047 g) in CO oxidation (20 ml/min, 1 vol% CO, $O_2/CO = 5$) at 303 K.

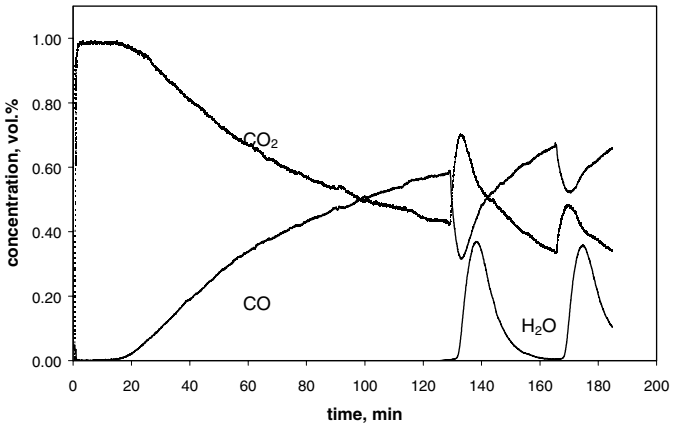

FIG. 7. Effect of the pulse injection of water vapor on the CO conversion (20 ml/min, 1 vol% CO, $O_2/CO = 5$) over the 1.3% $Au/FeO_x/ACF$ catalyst (0.047 g) at 303 K.

formed in the reaction of hydrogen oxidation can be adsorbed in the form of hydroxyl groups influencing the activity of the $Au/FeO_x/ACF$ catalyst. To check this, two consecutive pulses of water vapor were introduced during the reaction run (Fig. 7).

It is seen in Fig. 7 that water vapor provides the same effect as hydrogen, resulting in the increased conversion. This increase is reversible. The removal of water from the gas flow leads to the same conversion values as without water (Fig. 7). These results are in agreement with the data obtained for different gold catalysts on oxide/hydroxide supports (9, 10, 37, 48).

The water-promoting effect may be explained by modification of the catalyst surface or direct participation in the catalytic cycle (2, 48). However, direct or reversed water–gas shift reactions hardly can contribute in the water effect at low temperatures, since the rates of these reactions are normally several orders of magnitude lower than the rate of CO oxidation by oxygen (5). Water-promoted decomposition of carbonate species blocking active sites is also not justified, because no change in the C-balance was observed during the catalyst treatment by water vapor.

It is shown above that both hydrogen and water promote the CO oxidation. This result is in line with the data reported for the doped Au/Al_2O_3 (9).

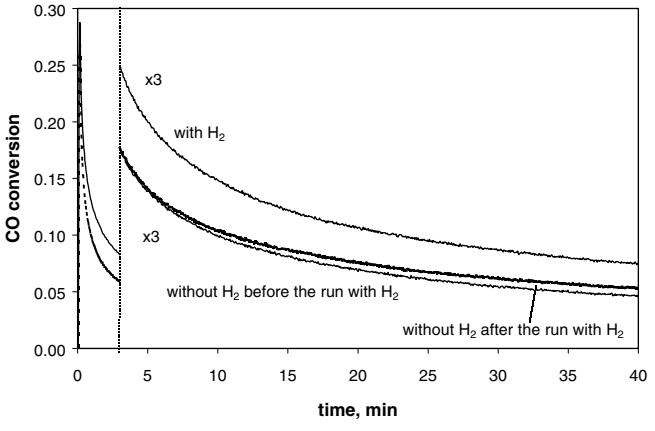

FIG. 6. Activity of the prereduced 1.3% $Au/FeO_x/ACF$ catalyst (0.02 g) at 303 K in the presence of hydrogen (1 vol% CO, 1 vol% O_2, 49 vol% H_2, 49 vol% He, 20 ml/min) and without it (1 vol% CO, 1 vol% O_2, 49 vol% Ar, 49 vol% He, 20 ml/min).

3.4. Morphological Properties of $Au/FeO_x/ACF$ Catalysts and Structure–Activity Relationship

It is known that the reactivity of Au-supported catalysts depends on the Au particle size and on the nature of the support (1, 4). The support may influence the Au particle-size distribution through such parameters as the Au diffusion rate and the density of nucleation sites on the surface. The CO oxidation reaction requires an optimal size of gold particles, in the range of 2–4 nm, as was the case for the Au/TiO_2 and Au/FeO_x catalysts (1, 4, 40). The gold clusters with a size less than 3 nm supported on TiO_2 loose their metallic character, which is essential for CO activation (49). A similar phenomenon is observed for gold clusters with the size of <2 nm supported on graphite surface (50).

The latest results give evidence that the interaction between the support and gold particles determines the catalyst performance (4). The role of the oxide support is assigned to the activation of O_2 (31) as well as to the formation of the Au/support interface (4). A model is suggested, in which CO is adsorbed on metallic Au or the Au/support perimeter interface and is oxidized by an active O species from the support (2, 4, 9, 32). Therefore, the determination of the size of Au particles and its dependence on the ACF modification by iron oxide is important. Special attention was paid to the elucidation of the Au particle location (on FeO_x particles or on the ACF surface).

TABLE 2

HRTEM-EDS Data on the Size of Gold and Iron Oxide Particles and Their Morphological Properties

Catalyst	Au particle size (nm) (maximal/typical/minimal)	Iron oxide particle size (nm) (maximal/typical/minimal)
0.12% Au/ACF	Bimodal: 50/30 and 5.0/2.5	—
0.5% Au/FeO_x/ACF (1.8% Fe)	40/5.0/2.0	15/3.0/1.5 Particle agglomeration
1.3% Au/FeO_x/ACF (4.5% Fe)	18/5.0/1.5	10/3.0/1.5 Particle agglomeration and Layered structure

An overview of the HRTEM-EDS study of different catalysts after CO oxidation is presented in Table 2. The 0.12% Au/ACF sample contains gold particles with typical mean sizes of 5 and 30 nm. A bimodal metal particle-size distribution was observed after Au deposition from $HAuCl_4$ solution on activated carbon (51). Such distribution of metal particles may be explained by the presence of different surface functional groups on the AC (23, 24). The acidic carboxylic –COOH groups in aqua media may provide a fast adsorption of $Au(en)_2^{3+}$ cations followed by their reductive decomposition with the formation of metallic gold.

The $Au(en)_2^{3+}$ cations interacting with less acidic surface groups are left intact on the support and are reduced later during the catalyst heating in hydrogen up to 573 K. It is clear that during the reductive heating of the catalysts the sintering of Au clusters will occur. Two main mechanisms of metal particles sintering on the supports are known: (i) agglomeration due to atom/clusters diffusion along the support, and (ii) Ostwald ripening, where large particles grow at the expense of smaller particles due to the atomization and diffusion between particles. The latter mechanism promoted by oxygen was shown to take place for the Au/TiO_2 system even at room temperature (40). Both mechanisms depend on the concentration of the nucleation centers, on metal loading, on the rate of surface diffusion, and on the reaction medium. The rate of surface diffusion at 573 K should be appreciable since this temperature is close to the Tammann temperature for dispersed gold (49).

The modification of ACF by iron oxide results in a decrease in the gold particle size (Table 2), even though the coverage of the support by iron oxide is relatively small (0.18–0.45 Fe atom nm^{-2}). This effect may be due to the order of the deposition steps of Fe^{3+} and $Au(en)_2^{3+}$ cations. Since first the adsorption of Fe^{3+} cations from aqueous solution occurred, the hydrophilic groups (strong acidic –COOH) on the ACF surface were blocked and/or destroyed (52). During the second step—adsorption of the $Au(en)_2^{3+}$ cations—only the less acidic groups are available. These sites are also known (24) as anchoring centers, hindering agglomeration and surface diffusion of metal atoms/particles. Thus, the modification of the ACF surface by iron oxide results in the decrease of the surface acidity diminishing the concentration of reductive centers for Au nucleation, leading to the formation of smaller gold particles. This is in accordance with a conclusion (24) that mildly acidic and more thermally stable oxygen species on the carbon surface are efficient barriers to metal particle growth and are thus beneficial for high metal dispersion.

EDS analysis was performed from different places numbered on the HRTEM image (Fig. 8). The relative Au and Fe atomic concentrations obtained from these places are presented in the form of a bar diagram (Fig. 8). The determined

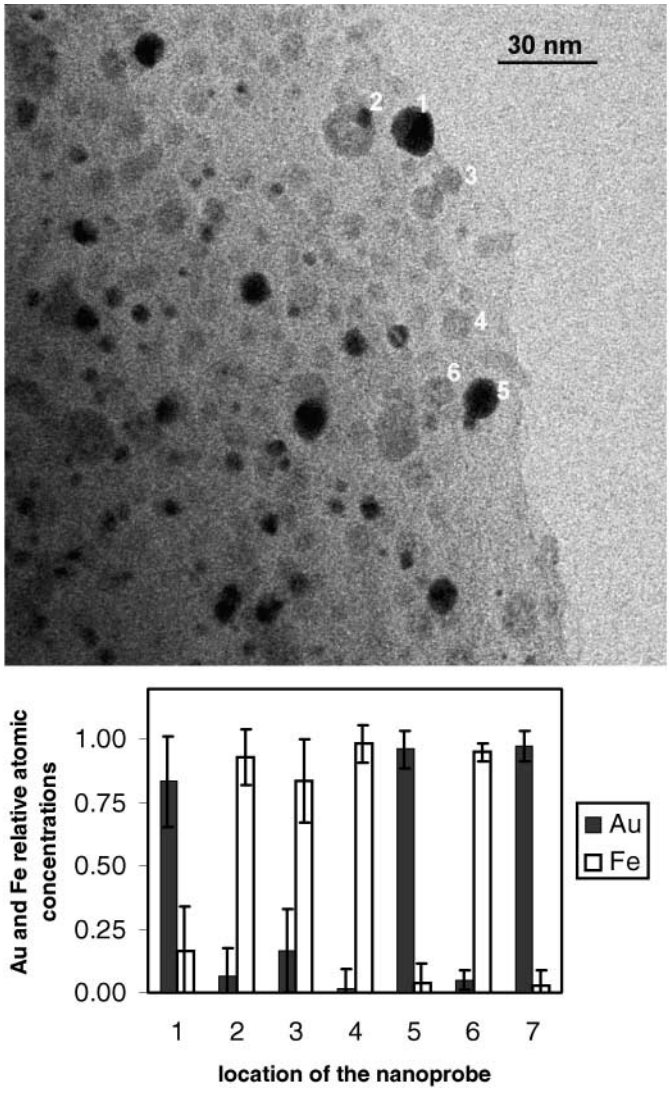

FIG. 8. Au and Fe relative atomic concentrations determined by EDS from the numbered places on the HRTEM image of 1.3% Au/FeO_x/ACF catalyst (Fe, 4.5%) after CO oxidation (the location of nanoprobe 7 is presented in Fig. 9).

concentration of the minor element in each particle is always below the statistical uncertainty. However, sometimes Au and Fe were found by EDS together in the same probe. For these cases it was confirmed by stereo microscopy (53) that this result is due to an accidental superposition of the projections from distinct particles of iron oxide and gold.

Hence, gold is present in the form of 3D-rounded particles (Figs. 8 and 9) distributed over the AC surface, but not on the iron oxide surface. The diffractogram of the Au particle (Fig. 9) corresponds to the crystal lattice of pure gold. However, the formation of surface gold oxide species (AuO_x) (40, 41, 44) could not be excluded as one of the reasons of deactivation.

The state of iron oxide may be also of importance for the catalyst activity since the strong dependence of the activity on the iron oxide concentration is observed. In the present work, the morphology of iron oxide in the Au/FeO_x/ACF catalysts after the reaction and contact with ambient air were studied by HRTEM-EDS. The diffractograms establish unambiguously the presence of Fe_2O_3 in the particles. The size of iron oxide particles was less than 15 nm for the catalysts with 1.8 and 4.5 wt% Fe (Table 2). For both samples the agglomerates of Fe_2O_3 particles are found. The main difference is that in the sample with the higher iron content, the additional formation of a layered structure of iron oxide is observed (Fig. 10). The diffractogram confirms the presence of Fe_2O_3 seen along the [8 4 1] orientation (Fig. 10).

It was found by EXAFS (54) that while the interatomic distances in iron oxide supported on coal were similar to the bulk phase, the coordination numbers of the iron neighbor shells were decreased. If the activation of oxygen takes place on iron oxide, this may be of importance for the catalytic activity. The modification of the ACF by iron oxide influences strongly the catalytic properties, providing a very high activity at a certain optimal concentration of iron (Table 1). The origin of the optimal concentration of iron evidently requires further study since the catalytic performance is dependent not only on the size of gold particles. The catalyst modified with iron oxide containing smaller gold particles (1.3% Au/FeO_x/ACF; Table 2) shows a lower activity in CO oxidation (Table 1) than the 0.5% Au/FeO_x/ACF catalyst with slightly bigger Au particles. The weak point of the obtained structural data for Au-supported catalysts is that the majority studies were performed not under *in situ* conditions (2) but in air containing water vapor. The contact with air implies the oxidation of reduced iron species (Fig. 4).

It was reported earlier that the reduction at 673 K of the FeO_x supported on AC gives metallic iron (55). Therefore, the reductive pretreatment of Au catalysts at 573 K used in this study provides partial Fe_2O_3 reduction. The *in situ* studies could be useful for better understanding of catalysis on the prereduced samples with respect to the preoxidized ones (Fig. 3).

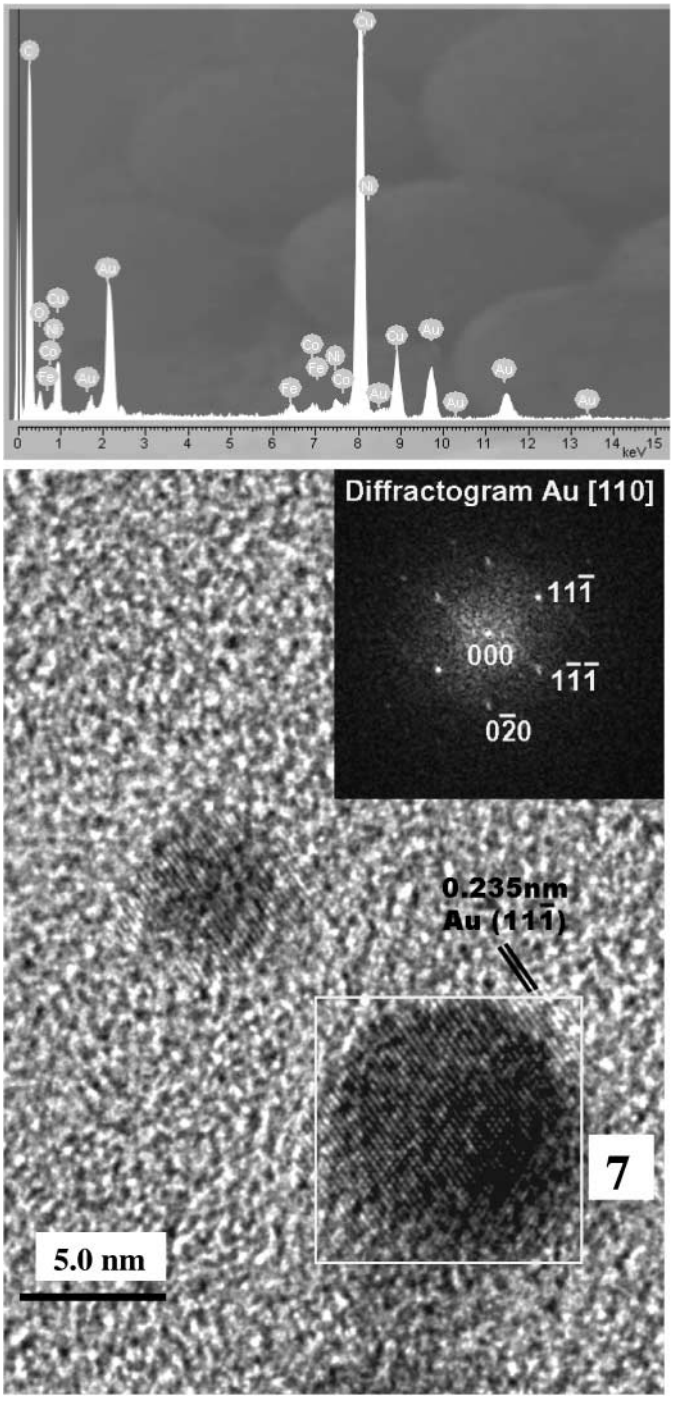

FIG. 9. HRTEM image, diffractogram, and ED spectrum from the zone surrounded by a square of the 1.3% Au/FeO_x/ACF catalyst (Fe, 4.5%) after CO oxidation (the Au and Fe relative atomic concentrations from the location of nanoprobe 7 are presented in Fig. 8).

The explanation of the iron oxide effect is closely connected with the question of the mechanism of the reaction. At present, it is not clear whether activation of both oxygen and CO take place on the finely dispersed gold, or if gold

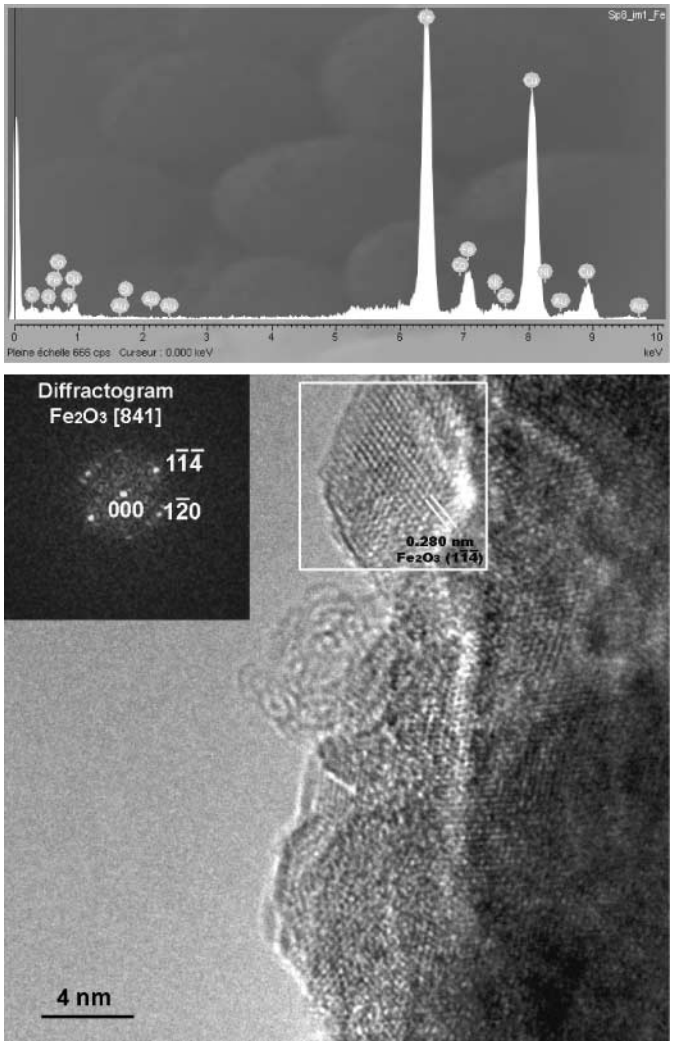

FIG. 10. The 1.3% Au/FeO_x/ACF catalyst (Fe, 4.5%) after CO oxidation: HRTEM image, diffractogram, and ED spectrum from the zone surrounded by the square.

activates only CO. The oxygen may be activated on the support with participation of iron-containing species followed by spillover to gold particles. The interaction of the two adsorbed species could take place on the gold/support interface determined by the size of Au particles (2–4).

4. CONCLUSIONS

1. Innovative structured catalysts based on Au nanoparticles supported on activated carbon fibers (ACF) in the form of woven fabrics were developed for low-temperature CO oxidation. Gold was deposited by adsorption from aqueous solution of ethylenediamine complex $[Au(en)_2]Cl_3$ followed by reduction in hydrogen.

2. In the Au/ACF catalyst, gold was found by HRTEM-EDS in the metallic state in the form of particles with sizes ranging from ~2.5–5 to ~30–50 nm.

3. A modification of the ACF by iron oxide was beneficial for the Au dispersion and catalytic activity. At low content, iron oxide was present on the ACF surface in the form of highly dispersed Fe_2O_3 particles and their agglomerates with 2- to 15-nm size. At higher Fe concentrations the formation of a layered structure of Fe_2O_3 was also observed. The peculiarities of this morphology are assigned to the decrease in the surface acidity of the ACF support due to FeO_x predeposition, which diminishes the concentration of reductive centers and hinders the sintering of Au during the heating in hydrogen.

4. Gold particles in the Au/FeO_x/ACF samples were not found to be in direct contact with the Fe_2O_3 phase and their size was smaller than without doping by iron oxide.

5. A reductive pretreatment is required for the activity of the Au/FeO_x/ACF catalysts, and the introduction of hydrogen (49 vol%) into the reaction mixture (CO and O_2) increases the catalytic activity, similarly to the water vapor addition. The activity of Au catalysts was drastically decreased in an oxygen-containing atmosphere due to the catalyst oxidation and carbonate/formate formation.

6. The CO oxidation activity of the Au/FeO_x/ACF catalysts at room temperature was higher compared to the granulated catalysts, such as Au/Al_2O_3 and Au/FeO_x/Al_2O_3, while no activity was found for the FeO_x/ACF catalyst.

ACKNOWLEDGMENTS

The authors thank the Swiss Commission of Technology and Innovation (CTI, Bern) for the financial support in the framework of TOPNANO 21 program. The work of Ms. A. Udriot for the chemical analysis and Mr. E. Casali for the SSA measurements is highly appreciated. Prof. B. E. Nieuwenhuys is gratefully acknowledged for valuable discussions.

REFERENCES

1. Haruta, M., *Catal. Today* **36**, 153 (1997).
2. Bond, G. C., and Thompson, D. T., *Gold Bull.* **33**, 41 (2000).
3. Bond, G. C., and Thompson, D. T., *Catal. Rev.–Sci. Eng.* **41**, 319 (1999).
4. Haruta, M., and Date, M., *Appl. Catal. A* **222**, 427 (2001).
5. Kahlich, M. J., Gasteiger, H. A., and Behm, R. J., *J. Catal.* **182**, 430 (1999).
6. Bethke, G. K., and Kung, H. H., *Appl. Catal. A* **194**, 43 (2000).
7. Schubert, M. M., Kahlich, M. J., Gasteiger, H. A., and Behm, R. J., *J. Power Sources* **84**, 175 (1999).
8. Trimm, D. L., and Onsan, Z. I., *Catal. Rev.* **43**, 31 (2001).
9. Grisel, R. J. H., and Nieuwenhuys, B. E., *J. Catal.* **199**, 48 (2001).
10. Haruta, M., Ueda, A., Tsubota, S., and Sanchez, R. M. T., *Catal. Today* **29**, 443 (1996).
11. Kiwi-Minsker, L., Yuranov, I., Slavinskaia, E., Zaikovskii, V., and Renken, A., *Catal. Today* **59**, 61 (2000).
12. Kiwi-Minsker, L., Yuranov, I., Siebenhaar, B., and Renken, A., *Catal. Today* **54**, 39 (1999).
13. Louis, B., Tezel, C., Kiwi-Minsker, L., and Renken, A., *Catal. Today* **69**, 365 (2001).
14. Kiwi-Minsker, L., Yuranov, I., Holler, V., and Renken, A., *Chem. Eng. Sci.* **54**, 4785 (1999).
15. Holler, V., Yuranov, I., Kiwi-Minsker, L., and Renken, A., *Catal. Today* **69**, 175 (2001).

16. Perez, M. M. C., Martinez de Lecea, S. C., and Solano, L. A., *Appl. Catal. A* **151**, 461 (1997).
17. Joannet, E., Horny, C., Kiwi-Minsker, L., and Renken, A., *Chem. Eng. Sci.*, in press.
18. Yoshikawa, M., Yasutake, A., and Mochida, I., *Appl. Catal. A* **173**, 239 (1998).
19. Nkosi, B., Coville, N. J., Hutchings, G. J., Adams, M. D., Friedl, J., and Wagner, F. E., *J. Catal.* **128**, 366 (1991).
20. Bianchi, C., Porta, F., Prati, L., and Rossi, M., *Top. Catal.* **13**, 231 (2000).
21. Prati, L., and Martra, G., *Gold Bull.* **32**, 96 (1999).
22. Block, B. P., and Bailar, J. C., *J. Am. Chem. Soc.* **73**, 4722 (1951).
23. Schlögl, R., *in* "Carbons" (G. Ertl, H. Knozinger, and J. Weitkamp, Eds.), p. 150. Wiley–VCH, Weinheim, 1999.
24. Radovic, L. R., and Rodriguez-Reinoso, F., *in* "Carbon Materials in Catalysis" (P. A. Thrower, Ed.), Vol. 25, p. 243. Dekker, New York, 1997.
25. Stadelmann, P., Jems Web Site. Available at http://cimewww.epfl.ch/people/Stadelmann/jemsWebSite/jems.html; CIME-EPFL: Lausanne, 2001.
26. "Inorganic Crystal Structure Database." FIZ Karlsruhe and Gmelin-Institute, Karlsruhe, 1997.
27. Sing, K. S. W., Everett, D. H., Haul, R. A. W., Moscou, L., Pierotti, R. A., Rouquerol, J., and Siemieniewska, T., *Pure Appl. Chem.* **57**, 603 (1985).
28. Krishnankutty, N., and Vannice, M. A., *Chem. Mater.* **1995**, 754 (1995).
29. Olea, M., Kunitake, M., Shido, T., and Iwasawa, Y., *Phys. Chem. Chem. Phys.* **3**, 627 (2001).
30. Liu, H. C., Kozlov, A. I., Kozlova, A. P., Shido, T., and Iwasawa, Y., *Phys. Chem. Chem. Phys.* **1**, 2851 (1999).
31. Okumura, M., Coronado, J. M., Soria, J., Haruta, M., and Conesa, J. C., *J. Catal.* **203**, 168 (2001).
32. Liu, H., Kozlov, A. I., Kozlova, A. P., Shido, T., Asakura, K., and Iwasawa, Y., *J. Catal.* **185**, 252 (1999).
33. Grisel, R. J. H., and Neiuwenhuys, B. E., *Catal. Today* **64**, 69 (2001).
34. Haruta, M., Tsubota, S., Kobayashi, T., Kageyama, H., Genet, M. J., and Delmon, B., *J. Catal.* **144**, 175 (1993).
35. Yuan, W. K., Kozlova, A. P., Wan, H., Tsai, K., and Iwasawa, Y., *J. Catal.* **170**, 191 (1997).
36. Kozlov, A. I., Kozlova, A. P., Liu, H. C., and Iwasawa, Y., *Appl. Catal. A* **182**, 9 (1999).
37. Park, E. D., and Lee, J. S., *J. Catal.* **186**, 1 (1999).
38. Knell, A., Barnickel, P., Baiker, A., and Wokaun, A., *J. Catal.* **137**, 306 (1992).
39. Bollinger, M. A., and Vannice, M. A., *Appl. Catal. B* **8**, 417 (1996).
40. Lai, X., and Goodman, D. W., *J. Mol. Catal. A* **162**, 33 (2000).
41. Minico, S., Scire, S., Crisafulli, C., Visco, A. M., and Galvagno, S., *Catal. Lett.* **47**, 273 (1997).
42. Grisel, R. J. H., Slyconish, J. J., and Nieuwenhuys, B. E., *Top. Catal.* **16**/**17**, 425 (2001).
43. Haruta, M., Yamada, N., Kobayashi, T., and Iijima, S., *J. Catal.* **115**, 301 (1989).
44. Chang, C.-K., Chen, Y.-J., and Yeh, C.-T., *Appl. Catal. A* **174**, 13 (1998).
45. Wagner, F. E., Galvagno, S., Milone, C., Visco, A. M., Stievano, L., and Calogero, S., *J. Chem. Soc. Faraday Trans.* **93**, 3403 (1997).
46. Finch, R. M., Hodge, N. A., Hutchings, G. J., Meagher, A., Pankhurst, Q. A., Siddiqui, M. R. H., Wagner, F. E., and Whyman, R., *Phys. Chem. Chem. Phys.* **1**, 485 (1999).
47. Visco, A. M., Neri, F., Neri, G., Donato, A., Milone, C., and Galvagno, S., *Phys. Chem. Chem. Phys.* **1**, 2869 (1999).
48. Cunningham, D. A. H., Vogel, W., and Haruta, M., *Catal. Lett.* **63**, 43 (1999).
49. Chusuei, C. C., Lai, X., Luo, K., and Goodman, D. W., *Top. Catal.* **14**, 71 (2001).
50. Rao, C. N. R., Santra, A. K., and Vijayakrishnan, V., *Top. Catal.* **1**, 25 (1994).
51. Riello, P., Canton, P., and Benedetti, A., *Langmuir* **14**, 6617 (1998).
52. Uchida, M., Shinohara, O., Ito, S., Kawasaki, N., Nakamura, T., and Tanada, S., *J. Colloid Interface Sci.* **224**, 347 (2000).
53. Reimer, L., *in* "Transmission Electron Microscopy," p. 255. Springer-Verlag, New York, 1993.
54. Huffman, G. P., Ganguly, B., Zhao, J., Rao, K., Shah, N., Feng, Z., Huggins, F. E., Taghiei, M. M., Lu, F. L., Wender, I., Pradhan, V. R., Tierney, J. W., Seehra, M. S., Ibrahim, M. M., Shabtai, J., and Eyring, E. M., *Energy Fuels* **7**, 285 (1993).
55. Jung, H.-J., Vannice, M. A., Mulay, L. N., Stanfield, R. M., and Delgass, W. N., *J. Catal.* **76**, 208 (1982).